



[Hassouna, S.](#), [Jamshed, M. A.](#), [Ur-Rehman, M.](#) , [Imran, M. A.](#) and [Abbasi, Q. H.](#) (2023) Investigating the Data Rate of Intelligent Reflecting Surfaces with Mutual Coupling and EMI. In: IEEE Wireless Communications and Networking Conference (WCNC2023), Glasgow, Scotland, UK, 26-29 March 2023, ISBN 9781665491228 (doi: [10.1109/WCNC55385.2023.10118853](https://doi.org/10.1109/WCNC55385.2023.10118853))

There may be differences between this version and the published version.
You are advised to consult the published version if you wish to cite from it.

<https://eprints.gla.ac.uk/287646/>

Deposited on 12 December 2022

Enlighten – Research publications by members of the University of Glasgow

<http://eprints.gla.ac.uk>

Investigating the Data Rate of Intelligent Reflecting Surfaces with Mutual Coupling and EMI

Saber Hassouna*, Muhammad Ali Jamshed*, Masood Ur-Rehman*, Muhammad Ali Imran*, and Qammer H. Abbasi*

* James Watt School of Engineering, University of Glasgow, Glasgow, U.K

Email: s.hassouna.1@research.gla.ac.uk

{ muhammadali.jamshed, masood.urrehman, muhammad.imran, qammer.abbasi } @glasgow.ac.uk

Abstract—In wireless communications, various study findings have shown that a reconfigurable intelligent surface (RIS) may successfully alter wireless wave parameters like phase and amplitude without requiring sophisticated signal processing and decoding at the receiver. However, it is necessary to take into account designing the surface under a realistic frequency selective fading channel. Because of this, we chose a wideband OFDM multi-user communication system based on an actual RIS setup that considers mutual coupling (MC) and electromagnetic interference (EMI). We used Hadamard matrix in the pilot transmissions to estimate the uncontrollable and the controllable channels. The best pilot configuration was selected to initialize the gradient descent method in order to calculate the optimal reflection coefficient that maximize the data rate for each user in the presence of EMI and MC. Simulation results revealed that the data rate has been degraded when considering EMI and MC for around 30 Mbits/s for each user. This confirms that both EMI and MC must be given considerable attention in our research due to their inevitable effects on the system performance.

Index Terms—Reconfigurable Intelligent Surface (RIS), Orthogonal Frequency Division Multiplexing (OFDM), Reflection Coefficient, Mutual Coupling (MC) and Electromagnetic Interference (EMI)

I. INTRODUCTION

Reconfigurable intelligent surfaces (RISs) are a recent innovation in the field of wireless communication research. The RISs are electromagnetically produced intelligent surfaces. Microelectronic circuits that are capable of wireless communication are used to regulate the materials and handling wireless propagation scenarios in a manner that was not before known [1], [2]. The RISs are made up of many tiny, inexpensive passive components (elements) that may be used to change wireless waves that impinge on them in ways that ordinary substances and materials cannot. It is important to note that prior research primarily focused on frequency flat fading channels for narrowband communications, where the reflection coefficients of the RIS are intended to modify the phase of the BS-RIS-User reflected path with the BS-User direct path for constructive interference. The RIS reflection coefficients must, however, account for all signal paths at varying delays when channels with frequency-selective fading nature are present, making optimization challenges more difficult to resolve. In contrast, several subcarriers in OFDM systems favour various configurations over a single one, which reduces the effective-

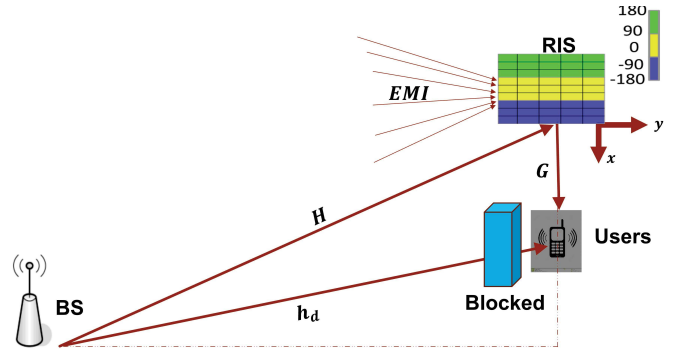


Fig. 1. The simulation setup for Multi-Users OFDM aided RIS

ness of RIS [2]. Heuristic techniques of various complexity are proposed in [3]–[5] for coupled channel estimation and RIS configuration in OFDM setups.

However, high percentage of the previous works did not take into consideration the effects of mutual coupling (MC) and electromagnetic interference (EMI) on RIS performance. According to our knowledge, we notice that the literature is lacking such important parameters and most of the research obtained results are overoptimistic. We have investigated RIS setup to look at the effect on the information rate for both the users who have line of sight (LOS) and the Non-(LOS) users under MC and EMI in a single-input-single-output (SISO) multi-user OFDM communication Setup. We developed the gradient descent method to reach to the optimal pilot configuration for each user. Simulation results revealed the gap in performance between the ideal case (when there is no EMI and MC) and the case when they have effect on the system setup. A summary of the remaining of this work is given as following, the system model is introduced in Section II. The EMI and channel model is the focus of Section III, while section IV present the phase shift model that is realistic. We show the pilot transmission and channel estimation in section V. sections VI and VII depict the dataset and the simulation outcomes, respectively. Finally, in part VIII, a conclusion is given.

II. SYSTEM MODEL

We take into account an OFDM-based multi-user wireless system where a RIS is used to improve communication between a base station (BS) and a user, as shown in Fig. 1. We assume for the sake of explanation that both the BS and the user are outfitted with a single antenna. It is considered that the RIS consists of N passive reflecting elements which is organized into a homogeneous planar array with horizontal row elements $N_H = 64$ and vertical column elements $N_V = 64$. The system's entire bandwidth is evenly split into K orthogonal subcarriers (SCs), similar to a typical OFDM-based system. All subcarriers' power distributions P_0, \dots, P_{K-1} fulfil $P = \frac{1}{K} \sum_{k=0}^{K-1} p_k$ where $p_k = E\{|\bar{x}[k]|^2\}$ is the power given to subcarrier v . Let the direct channel $h_d = [h_d[0], \dots, h_d[M-1]]^T \in \mathbb{C}^{M \times 1}$ describes all the direct (uncontrollable) channel coefficients. Additionally, there is a M -tap baseband equivalent multipath channel for the BS-RIS-user link via which the RIS reflects the signal that the BS transmits before it reaches the users consequently, let $H = [h_0, \dots, h_{M-1}] \in \mathbb{C}^{N \times M}$ is the BS-RIS channel where $h_l \in \mathbb{C}^{N \times 1}$ corresponds to the l -th tap, $0 \leq l \leq M-1$ while $G = [g_0, \dots, g_{M-1}] \in \mathbb{C}^{N \times M}$ is the RIS-User channel where $g_l^H \in \mathbb{C}^{1 \times N}$ corresponds to the l -th tap, $0 \leq l \leq M-1$. When the signal is received at the RIS, each element re-scatters it with a different reflection coefficient so, $w_\theta = \text{diag}(e^{j\theta_1}, e^{j\theta_2}, \dots, e^{j\theta_N})$ is the diagonal matrix that contains the reflection coefficients of the RIS. For the sake of clarity, let us denote $V = [v_0, \dots, v_{M-1}] \in \mathbb{C}^{N \times M}$ where $v_l^H = g_l^H \text{diag}(h_l) \in \mathbb{C}^{1 \times N}$. Then we have $v_l^H w_\theta = g_l^H w_\theta h_l$ that characterizes the BS-RIS-User composite channel at the l -th tap. The received signal $z_k \in \mathbb{C}$ at the k -th subcarrier $k = 0, \dots, K-1$ using the discrete Fourier transform (DFT) at the RIS is given [6]:

$$z_k = H_k x_k + e_{EMI}, \quad (1)$$

where, x_k is the transmitted signal and $e_{EMI} \in \mathbb{C}^N$ is the EMI produced by the incoming uncontrollable waves. The received signal $r_k \in \mathbb{C}$ at the receiver is given as per Fig. 1:

$$r_k = z_k w_\theta G_k^H + h_d x_k + e_k, \quad (2)$$

where, $e_k \sim \mathcal{N}_{\mathbb{C}}(0, \sigma_e^2)$ is the receiver noise affecting the wave reception except for the EMI reflected by the RIS. By substituting (1) in (2).

$$r_k = (G_k^H w_\theta H_k + h_d) x_k + w_\theta G_k^H e_{EMI} + e_k. \quad (3)$$

Let us denote $h_\theta = (G_k^H w_\theta H_k + h_d)$ and $\mathcal{G} = w_\theta G_k^H$. We can represent (3) in a vector form as follows:

$$\begin{bmatrix} \bar{r}[0] \\ \vdots \\ \bar{r}[K-1] \end{bmatrix} = \begin{bmatrix} \bar{h}_\theta[0] \\ \vdots \\ \bar{h}_\theta[K-1] \end{bmatrix} \odot \begin{bmatrix} \bar{x}[0] \\ \vdots \\ \bar{x}[K-1] \end{bmatrix} + \begin{bmatrix} \bar{\mathcal{G}}\bar{e}_{EMI}[0] \\ \vdots \\ \bar{\mathcal{G}}\bar{e}_{EMI}[K-1] \end{bmatrix} + \begin{bmatrix} \bar{e}[0] \\ \vdots \\ \bar{e}[K-1] \end{bmatrix}, \quad (4)$$

where, \odot denotes the Hadamard product. The output of the OFDM block can be described in a short form as follows:

$$\bar{r} = \bar{h}_\theta \odot \bar{x} + \bar{\mathcal{G}}\bar{e}_{EMI} + \bar{e}. \quad (5)$$

We notice that the channel frequency response of \bar{h}_θ is:

$$\bar{h}_\theta = F \begin{bmatrix} h_d[0] + v_0^H w_\theta \\ \vdots \\ h_d[M-1] + v_{M-1}^H w_\theta \end{bmatrix} = F (h_d + V^H w_\theta) \quad (6)$$

where, F is a $K \times M$ DFT matrix. At each k -th SC, the channel frequency response is characterised as follows:

$$h_{\theta_k} = f_k^H h_d + f_k^H V^H w_\theta, \quad k = 0, \dots, K-1, \quad (7)$$

where, f_k^H describes the k -th row of the DFT matrix F . Consequently for all subcarriers K with equal power distribution, we can represent the total sum information rate for a known w_θ configuration and complete channel knowledge as follows:

$$\mathcal{R} = \frac{B}{K+M-1} \sum_{k=0}^{K-1} \log_2 \left(1 + \frac{P |f_k^H h_d + f_k^H V^H w_\theta|^2}{A \sigma^2 \mathcal{G}^H R \mathcal{G} + \sigma_e^2} \right) \frac{\text{bit}}{s} \quad (8)$$

where, the total bandwidth is B , P is the radiated power in watt, M is the channel taps and the term $A \sigma^2 \mathcal{G}^H R \mathcal{G}$ is the interference term that will be considered as a noise in this paper.

III. EMI AND CHANNEL MODEL

A. EMI Model

A cline of incoming plane waves from external sources are superimposed to create the EMI e_{EMI} . The e_{EMI} is modelled as in [6] and distributed as $e_{EMI} \sim \mathcal{N}_{\mathbb{C}}(0, A \sigma^2 R)$ where A is the RIS element area, σ^2 is the interference variance and the (n, m) -th unit of R is given by:

$$[\mathbf{R}]_{n,m} = \iint_{-\pi/2}^{\pi/2} e^{j\mathbb{W}(\varphi, \theta)^T (\mathbf{u}_n - \mathbf{u}_m)} f(\varphi, \theta) d\varphi d\theta, \quad (9)$$

where, $\mathbb{W}(\varphi, \theta) = \frac{2\pi}{\lambda} [\cos(\theta) \cos(\varphi), \cos(\theta) \sin(\varphi), \sin(\theta)]^T$ is the wave number that describes the phase changes of the plane waves in relation to its three Cartesian coordinates. $f(\varphi, \theta)$ is the power angular density with $\iint_{-\pi/2}^{\pi/2} f(\varphi, \theta) d\varphi d\theta = 1$ and $\mathbf{u}_n = [0, i(n)d_v, j(n)d_h]^T$ is the location of the n -th element with $n \in [1, N]$. d_v and d_h are the vertical and horizontal elements spacing where, $d_v^2 = d_h^2 = A$ and $i(n)$ and $j(n)$ are the horizontal and vertical indices of element n . Under circumstances of isotropic distribution (i.e. uniform distribution from all angles), (9) can be reduced to [7]:

$$[R^{\text{iso}}]_{n,m} = \text{sinc} \left(\frac{2 \|\mathbf{u}_n - \mathbf{u}_m\|}{\lambda} \right), \quad (10)$$

where, $\|\cdot\|$ is the Euclidean norm.

B. Channel Model

The propagation models used in this research are more realistic because it considers multipath and can be represented by array response vectors rather than narrow flat fading channel. The channels are determined by the shape of the RIS and environment. Particularly, the wideband channel of [2] is implemented, where the BS-User direct uncontrollable link is given as:

$$h_d = \sum_{\ell=1}^{L_d} \sqrt{\beta_{d,\ell}} e^{-j2\pi f_c \tau_{d,\ell}} \begin{bmatrix} \text{sinc}(0 + B(\alpha - \tau_{d,\ell})) \\ \vdots \\ \text{sinc}(M-1 + B(\alpha - \tau_{d,\ell})) \end{bmatrix}, \quad (11)$$

where, L_d is the number of propagation paths, $B_{d,\ell} \geq 0$ is the pathloss of the l -th path, $\tau_{d,\ell}$ is the propagation delay and α is the sampling delay over the shortest path. Similarly, it is worth mentioning that explicit knowledge of individual channels h_l and g_l^H are not needed and the controllable composite link BS-RIS-User is given by:

$$V = \sum_{\ell=1}^{L_a} \sum_{\ell_b=1}^{L_b} \sqrt{\beta_{H,\ell} \beta_{G,\ell_b}} e^{-j2\pi f_c (\tau_{H,\ell} + \tau_{G,\ell_b})} a(\varphi_{H,\ell}, \theta_{H,\ell}) \odot a(\varphi_{G,\ell_b}, \theta_{G,\ell_b}) \begin{bmatrix} \text{sinc}(0 + B(\alpha - \tau_{H,\ell} - \tau_{G,\ell_b})) \\ \vdots \\ \text{sinc}(M-1 + B(\alpha - \tau_{H,\ell} - \tau_{G,\ell_b})) \end{bmatrix}^T \quad (12)$$

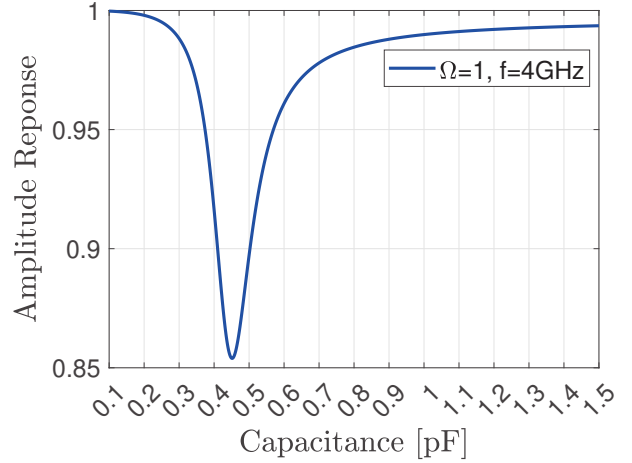
where, L_a and L_b are the propagation paths from the BS to the RIS and from the RIS to the users, respectively. $B_{H,\ell} \geq 0$, and $B_{G,\ell_b} \geq 0$, are the pathlosses from the BS to the RIS and from the RIS to the user, respectively. $\tau_{H,\ell}$ and τ_{G,ℓ_b} are the propagation delays to and from the RIS and $a(\varphi, \theta)$ is the array response vector with φ and θ are the azimuth and elevation angles. We perform pilot transmission in section V to estimate the channels h_d and V at the receiver however, accurate knowledge of the channel link G between the RIS and the users is needed to calculate the uncontrollable EMI so, we will assume the knowledge of G at the receiver. The simulations parameters are considered based on 3GPP channel models [8], [9].

IV. PRACTICAL PHASE SHIFT MODEL

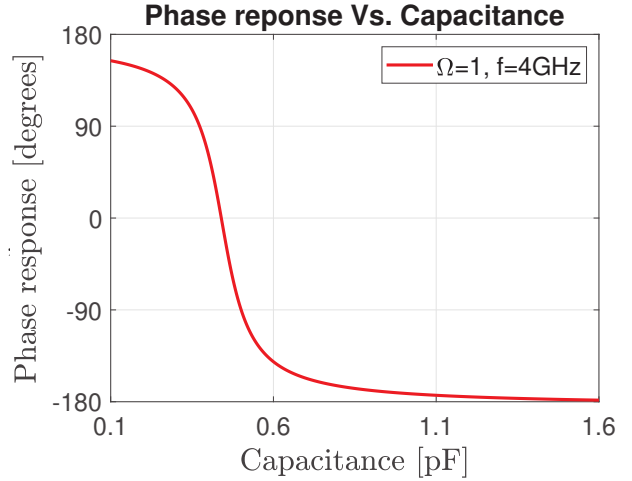
The corresponding model for the n -th reflecting element impedance is provided by [10]:

$$\mathbb{Z}_n(C_n, \Omega_n) = \frac{j2\pi f L_1 \left(j2\pi f L_2 + \frac{1}{j2\pi f C_n} + \Omega_n \right)}{j2\pi f L_1 + \left(j2\pi f L_2 + \frac{1}{j2\pi f C_n} + \Omega_n \right)}. \quad (13)$$

The bottom layer inductance, top layer inductance, effective capacitance, effective resistance, and carrier frequency of the incident signal are represented as L_1, L_2, C_n, Ω_n and f respectively. The reflection coefficient describes the portion of the reflected electromagnetic wave that is attributable to the



(a)



(b)

Fig. 2. a) Amplitude and b) Phase Responses versus C_n

discontinuity in impedance between the element $\mathbb{Z}_n(C_n, \Omega_n)$ and free space impedance \mathbb{Z}_o :

$$\Gamma_n = \frac{\mathbb{Z}_n(C_n, \Omega_n) - \mathbb{Z}_o}{\mathbb{Z}_n(C_n, \Omega_n) + \mathbb{Z}_o}. \quad (14)$$

Γ_n being a function of C_n, Ω_n and f , allows us to control and programme the reflected electromagnetic waves by changing the values of C_n, Ω_n and f . C_n has values that vary from 0.15 pF to 1.5 pF, $\Omega_n = 1$ ohm, $\mathbb{Z}_o = 377$, and $f = 4$ GHz. The RIS element will scatter a sinusoidal signal impinging at frequency f with an amplitude of $|\Gamma_n|$ and a phase shift of $\arg(\Gamma_n)$. For example, in the case of a one-bit RIS, one PIN diode is required per RIS element, and more diodes are needed for more resolution but at the cost of complex design. Consequently, the RIS is adjusted by using multiple PIN diodes numbers assigned to every element. Two alternative capacitance values can be used with each PIN diode. In this investigation, we look at the information rate

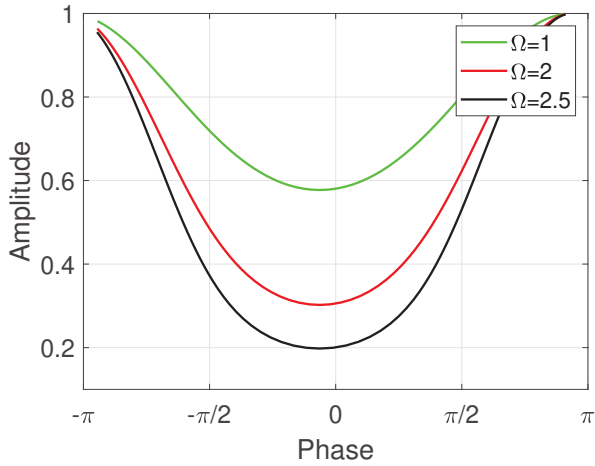


Fig. 3. Reflected amplitude vs. phase shift for RIS element

for users for different capacitance value pairs that correlate to varying reflecting phase shifts per RIS element. Fig. 2 illustrates the responses of amplitude and phase for different values of capacitances. It was found that because the amplitude response and phase shifts of the reflecting element are typically non-linearly linked, they cannot be controlled separately. The reflection amplitude, as illustrated in Fig. 3, achieves a modest value at phase shift equals zero, but it grows consistently as the phase shift reaches 180 or -180 and asymptotically approaches one. As a consequence, it is incorrect for many earlier research to assume that the amplitude response value is one.

The reflecting phase shift provided by each capacitance value varies. For instance, the capacitance values of 0.5011 pF and 0.3732 pF correspond to phases of -90 and 90 respectively, and will provide a 180 phase shift spacing per element. When RIS is included, the reflection coefficients can be expressed as follows [11]:

$$w_\theta = \begin{bmatrix} \Gamma(C_1, f) \\ \vdots \\ \Gamma(C_N, f) \end{bmatrix}, \quad (15)$$

where, $C_n \in \{C_1, \dots, C_N\}$ is the actual capacitance value of element n . We used the statistical correlation model of the coupling effect in [11] to study the effect of MC on the performance:

$$C_n = \sum_{i=1}^N C_{i,\theta} \frac{100^{-\frac{d_{n,i}}{\lambda}}}{\sum_{j=1}^N 100^{-\frac{d_{n,i}}{\lambda}}}, \quad (16)$$

where, $d_{n,i}$ is the distance between element n and element i , $C_{i,\theta}$ is the capacitance assigned to element i and λ is the wavelength. By examining the element in row 10 of column 10, the factor multiplied by $C_{i,\theta}$, in (16) for the various elements is shown in Fig. 4. We see that the assigned capacitance of the element and the intended capacitance of its neighbours both affect the actual capacitance to 45% and 55%,

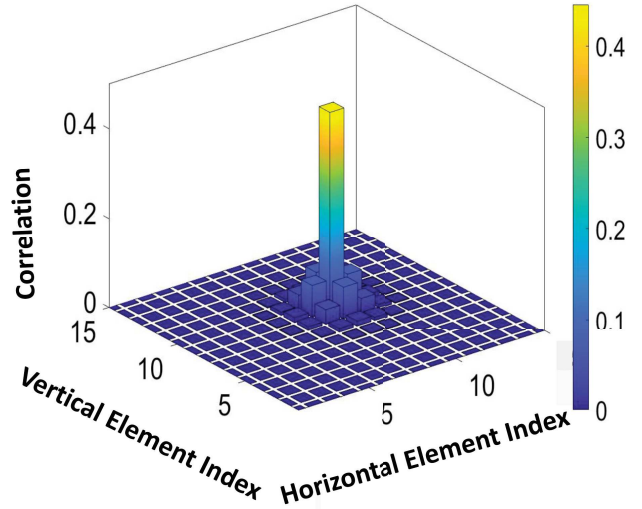


Fig. 4. The assigned capacitance of itself and its surrounding elements is correlated with the actual capacitance of the RIS element at row 10 and column 10.

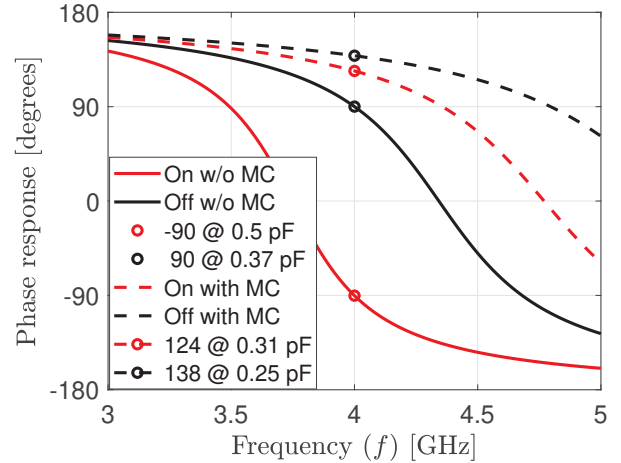


Fig. 5. The reflection coefficient phase response in (14) considering mutual coupling at 4GHz frequency.

respectively. The more closely two elements are together, the more they effect one another [11]. The effect of MC on the reflection coefficient phase response at the carrier frequency $f = 4$ GHz is illustrated in Fig. 5. The assigned capacitance value for the element is changed due to the MC effect and hence the corresponding phase is changed accordingly. For example in the case without MC, the assigned values of capacitance 0.37 pF and 0.5 pF are corresponding to phase shifts 90 and -90 degrees. However, when considering MC, the actual values of capacitance will be 0.31 pF and 0.25 pF and that lead to a deviation in the phase shifts from 90 and -90 degrees to 138 and 124 degrees. We will show the effect of the MC on the achievable data rate in the next sections.

V. PILOT TRANSMISSION AND CHANNEL ESTIMATION

The pilot signaling will be based on employing the columns of a Hadamard matrix \mathcal{H}_N , whose entries are either +1 or -1, with a scheme that makes the columns mutually orthogonal [5]. The received signal from the pilot transmission will be expressed as in [11] with extra step that add the EMI e_{EMI} in the received signal in addition to the receiver noise. EMI is seen as noise in the context of wireless communications due to the fact that EMI is produced by uncontrolled signals.

$$\begin{aligned} r &= xF(h_d[1, \dots, 1] + V^T[w_{\theta_1}, \dots, w_{\theta_N}]) + \mathcal{G}e_{EMI} + e \\ &= xF[h_d, V^T] \begin{bmatrix} 1, \dots, 1 \\ \mathcal{P} \end{bmatrix} + \mathcal{G}e_{EMI} + e \end{aligned} \quad (17)$$

where, $r = [\bar{r}_1, \dots, \bar{r}_N] \in \mathbb{C}^{N \times N}$ contains all the received signals, $\mathcal{G}e_{EMI} = [\bar{\mathcal{G}}e_{EMI_1}, \dots, \bar{\mathcal{G}}e_{EMI_N}] \in \mathbb{C}^{N \times N}$ is the interference matrix, $e = [\bar{e}_1, \dots, \bar{e}_N] \in \mathbb{C}^{N \times N}$ is the noise matrix and $\mathcal{P} = [w_{\theta_1}, \dots, w_{\theta_N}]$ gathers all the RIS configurations. The assigned matrix $\hat{\mathcal{P}} = \mathcal{P} + E$ where E is the unknown hardware mismatch. Let \dagger represents the Moore-Penrose inverse then the least square (LS) estimate of the received signal in (17) can be calculated as follows [2]:

$$\begin{aligned} \frac{1}{x} F^\dagger r \begin{bmatrix} 1, \dots, 1 \\ \hat{\mathcal{P}} \end{bmatrix}^\dagger &= [h_d, V^H] \begin{bmatrix} 1, \dots, 1 \\ \hat{\mathcal{P}} \end{bmatrix} \\ &\times \begin{bmatrix} 1, \dots, 1 \\ \hat{\mathcal{P}} \end{bmatrix}^\dagger + \underbrace{[h_d, V^H] \begin{bmatrix} 0, \dots, 0 \\ E \end{bmatrix} \begin{bmatrix} 1, \dots, 1 \\ \hat{\mathcal{P}} \end{bmatrix}^\dagger}_{\text{Hardware Mismatch}} \\ &+ \underbrace{\frac{1}{x} F^\dagger \mathcal{G}e_{EMI} \begin{bmatrix} 1, \dots, 1 \\ \hat{\mathcal{P}} \end{bmatrix}^\dagger}_{\text{Interference}} + \underbrace{\frac{1}{x} F^\dagger e \begin{bmatrix} 1, \dots, 1 \\ \hat{\mathcal{P}} \end{bmatrix}^\dagger}_{\text{Noise}}, \end{aligned} \quad (18)$$

where, $[h_d, V^H]$ is the desired channel term. The number of pilot signals is sufficient to obtain a unique LS estimate for the channel coefficients however we can reduce the dimension of the estimation problem by taking the advantage that the channel components within each column of the RIS are equal so, equation (17) can be expressed as:

$$r = xF[h_d, V_{row}^H] \begin{bmatrix} 1, \dots, 1 \\ \mathcal{A}^H \mathcal{P} \end{bmatrix} + \mathcal{G}e_{EMI} + e, \quad (19)$$

where, $\mathcal{A} = (1_{N_V} \otimes I_{N_H}) \in \mathbb{C}^{N \times N_H}$, is the projection matrix and \otimes denotes the Kronecker product. $V_{row} \in \mathbb{C}^{N_H \times M}$ is the reduced dimension channel coefficients for RIS rows. Consequently, it is possible to compute the LS estimate as follows:

$$\begin{bmatrix} \hat{h}_d, \hat{V}_{row}^T \end{bmatrix} = \frac{1}{x} F^\dagger r \begin{bmatrix} 1, \dots, 1 \\ \mathcal{A}^H \hat{\mathcal{P}} \end{bmatrix}^\dagger. \quad (20)$$

It is necessary to choose the most optimized vector $\hat{\mathcal{P}}$ in order to maximize \hat{h}_d and \hat{V}_{row}^T with regard to the RIS configurations. We must identify a considerable tradeoff among all K subcarriers to optimize the RIS. In the academia, there are

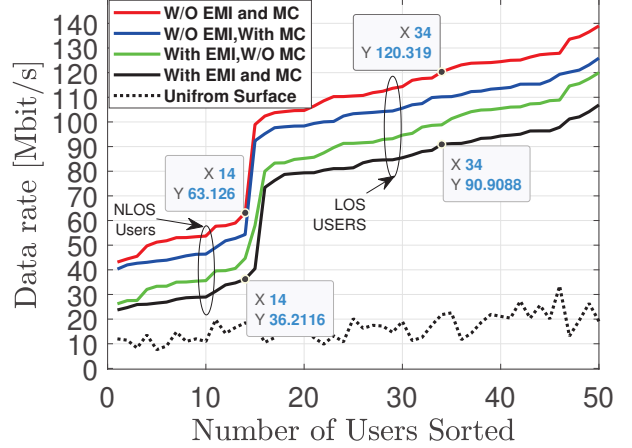


Fig. 6. The data rate achieved with the presence of both mutual coupling (MC) and the electromagnetic interference (EM).

Algorithm 1: Gradient descent method for optimizing the data rate \mathcal{R}

- 1: Select $w_{\theta_{\text{pilot}}} \in [w_{\theta_1}, \dots, w_{\theta_N}]$ from the received signal r in (17) that gives the maximum data rate in (8) and set $w_{\theta} = w_{\theta_{\text{pilot}}}$
- 2: Let $\mathcal{V} = [\hat{h}_d, \hat{V}_{row}^T]^H [\hat{h}_d, \hat{V}_{row}^T]$ and $\bar{a}_0 = \begin{bmatrix} 1 \\ w_{\theta_{\text{pilot}}} \end{bmatrix}$
- 3: Compute $\mathcal{V}\bar{a}_i$
- 4: Set $n = 1$
- 5: **for** $n < \text{Maximum number of iterations}$ **do**
- 6: set $\mu = \gamma/\lambda (\sqrt{\mathcal{V}^H} \sqrt{\mathcal{V}})$ with $\gamma \in [0, 1]$ [6] and λ is the wavelength
- 7: Update $\bar{a}_{i+1} = \bar{a}_i + \mu \mathcal{V}\bar{a}_i$
- 8: Set $a_{i+1} = e^{j \arg(\bar{a}_{i+1})}$
- 9: Rotate the solution to ensure that the 1st entry is 1 for the direct channel h_d (uncontrollable)
- 10: Quantize phases of a_{i+1} to be 1 or -1 to get the optimized $w_{\theta_{\text{pilot}}}$ vector.
- 11: **end for**
- 12: We get $w_{\theta_{\text{optimized}}}$
- 13: Evaluate the new data \mathcal{R}_{new} with $w_{\theta_{\text{optimized}}}$ according to (8) by setting $w_{\theta} = w_{\theta_{\text{optimized}}}$

heuristic methods that rely on successive convex approximation, semidefinite relaxation, and strongest tap maximization (STM) in the time domain [3], [4]. However, we will use the same methodology in [11] but the gradient descent instead of the power method in order to ensure that it works for LOS and NLOS channels as shown in Algorithm 1. The gradient descent method starts with the initial solution \bar{a}_0 and ending with calculating the optimized reflection coefficient vector w_{θ} for each user. The output of Algorithm 1 is to get the optimized $w_{\theta_{\text{optimized}}}$ in order to achieve the maximized information rate for each user.

VI. DATASET

We used the Dataset-2 of [11] which takes into account 50 users and contains N received OFDM signal blocks for each user obtained with the pilot transmission \hat{P} with additional modifications that include the EMI and MC. We considered the EMI term $w_{\theta} G_k^H e_{EMI}$ in (3) to the received signals of all 50 users to study the effect of interference on the information rate for users. Moreover, we set the correlation matrix in the Dataset-2 for the capacitance to unity matrix I_N to compare the achievable data rate with and without MC using the statistical model defined in (16).

VII. SIMULATION RESULTS

Figure 6 displays the data rates attained by the 50 users in various configuration scenarios. The case without EMI and MC is the reference that we will compare the other setups with. We investigated the effect of MC and EMI together and separately on the system performance and notice that the data rate is dramatically declined with the presence of both MC and EMI. We select user 14 among the NLOS users and user 34 from the LOS users to calculate the gap in the data rate between the ideal reference case and the case that includes both MC and EMI. We notice a degradation of 30 Mbits/s for each user and this confirms that MC and EMI are parameters that we should consider in RIS design especially when the surface is large which exactly corresponds to the situation when the RIS is most beneficial.

VIII. CONCLUSION

In this research, we demonstrated the effect of EMI and MC on the achievable data rate for each user. The pilot transmission is utilized to estimate the direct and the indirect channels. A gradient descent algorithm is developed to allocate the best and the high quality configuration to enhance the information rate per each LOS and NLOS user. Since RIS technology and 6G research are intertwined, it is now important to find improved communication models that can take advantage of electromagnetic characteristics and be compatible with practical applications.

REFERENCES

- [1] Q. Wu, S. Zhang, B. Zheng, C. You, and R. Zhang, "Intelligent reflecting surface-aided wireless communications: A tutorial," *IEEE Transactions on Communications*, vol. 69, no. 5, pp. 3313–3351, 2021.
- [2] E. Björnson, H. Wymeersch, B. Matthiesen, P. Popovski, L. Sanguinetti, and E. de Carvalho, "Reconfigurable intelligent surfaces: A signal processing perspective with wireless applications," *IEEE Signal Processing Magazine*, vol. 39, no. 2, pp. 135–158, 2022.
- [3] Y. Yang, B. Zheng, S. Zhang, and R. Zhang, "Intelligent reflecting surface meets ofdm: Protocol design and rate maximization," *IEEE Transactions on Communications*, vol. 68, no. 7, pp. 4522–4535, 2020.
- [4] B. Zheng and R. Zhang, "Intelligent reflecting surface-enhanced ofdm: Channel estimation and reflection optimization," *IEEE Wireless Communications Letters*, vol. 9, no. 4, pp. 518–522, 2019.
- [5] M. M. Amri, N. M. Tran, and K. W. Choi, "Reconfigurable intelligent surface-aided wireless communications: adaptive beamforming and experimental validations," *IEEE Access*, vol. 9, pp. 147 442–147 457, 2021.
- [6] A. de Jesus Torres, L. Sanguinetti, and E. Björnson, "Electromagnetic interference in ris-aided communications," *IEEE Wireless Communications Letters*, vol. 11, no. 4, pp. 668–672, 2021.
- [7] E. Björnson and L. Sanguinetti, "Rayleigh fading modeling and channel hardening for reconfigurable intelligent surfaces," *IEEE Wireless Communications Letters*, vol. 10, no. 4, pp. 830–834, 2020.
- [8] Spatial channel model for multiple input multiple output (mimo) simulations (release 16). [Online]. Available: <https://portal.3gpp.org/desktopmodules/Specifications/SpecificationDetails.aspx?specificationId=1382>
- [9] E. Björnson and L. Marcenaro, "Configuring an intelligent reflecting surface for wireless communications: Highlights from the 2021 ieee signal processing cup student competition [sp competitions]," *IEEE Signal Processing Magazine*, vol. 39, no. 1, pp. 126–131, 2021.
- [10] S. Abeywickrama, R. Zhang, Q. Wu, and C. Yuen, "Intelligent reflecting surface: Practical phase shift model and beamforming optimization," *IEEE Transactions on Communications*, vol. 68, no. 9, pp. 5849–5863, 2020.
- [11] E. Björnson, "Optimizing a binary intelligent reflecting surface for ofdm communications under mutual coupling," in *WSA 2021; 25th International ITG Workshop on Smart Antennas*. VDE, 2021, pp. 1–6.